Prediction of the *AU*, *AL*, and *AE* indices using solar wind parameters

Bingxian Luo,[1,2] Xinlin Li,[2] M. Temerin,[3] and Siqing Liu[1]

Received 2 July 2013; revised 1 November 2013; accepted 20 November 2013.

[1] An empirical model that predicts the *AU* index, a measure of the Earth's east electrojet, derived from magnetometers in the Northern Hemisphere, is introduced together with an improved *AL* model which, combined with the *AU* model, produces an *AE* model. All models are based on solar wind and interplanetary magnetic field parameters and the solar $F_{10.7}$ index for the years 1995 to 2001. The linear correlation coefficient (LC) between the 10 min averaged *AU* index and the model is 0.846 for the years 1995–2001. The LC for the updated *AL* model is 0.846, and using $AE = AU - AL$, the LC for the *AE* model is 0.888. The better LC of the *AE* model over *AU* and *AL* models is because *AU* and *AL* are better correlated than their errors. The models show that (1) solar ultraviolet intensity plays a significant role in auroral activity by changing the ionospheric conductivity and scale height. Increasing solar ultraviolet intensity increases the eastward electrojet as measured by *AU* but decreases the westward electrojet as measured by *AL*; (2) solar wind dynamic pressure also affects the auroral electrojet indices, although they are much more strongly dependent on the solar wind velocity and the interplanetary magnetic field; (3) *AU* and *AL* behave differently during geomagnetic storm main phases: *AU*, unlike *AL*, can drop to a small value during storms; (4) the longer averaged auroral electrojets indices can be predicted well but shorter timescale variations are less predictable.

Citation: Luo, B., X. Li, M. Temerin, and S. Liu (2013), Prediction of the *AU*, *AL*, and *AE* indices using solar wind parameters, *J. Geophys. Res. Space Physics*, *118*, doi:10.1002/2013JA019188.

1. Introduction

[2] The auroral electrojet indices *AU*, *AL*, and *AE* have been widely used for monitoring geomagnetic activity and space weather and for research in geomagnetism, aeronomy, and solar-terrestrial physics since their introduction by *Davis and Sugiura* [1966]. The *AU* and *AL* indices represent the strongest current intensities of the eastward and westward auroral electrojets, respectively, as measured by a select network of magnetometers in the auroral zone. The *AE* index, defined as the difference of *AU* and *AL*, $AE = AU - AL$, represents the overall activity of the electrojets.

[3] Though many uncertainties exist in the auroral electrojet indices [*Kamide and Rostoker*, 2004; *Li et al.*, 2007], the auroral electrojet indices are still widely used as a proxy for auroral activity. Many efforts have been made to understand their variability and predictability. It has been demonstrated that the auroral electrojet indices have strong universal time [*Davis and Sugiura*, 1966; *Ahn et al.*, 2000a], seasonal [*Russell and McPherron*, 1973; *Ahn et al.*, 2000b; *Cliver et al.*, 2000; *Lyatsky et al.*, 2001], annual [*Lyatsky et al.*, 2001; *Pulkkinen et al.*, 2011], and solar cycle [*Ahn et al.*, 2000b] variation. It has been claimed that *AU* and *AL* have different driving forces and that *AU* reflects mainly the directly driven component of auroral activity, while *AL* contains significant contributions from both directly driven and substorm expansion phase activity [*Allen and Kroehl*, 1975].

[4] Others have tried to model the indices in different ways, such as through dynamic systems [*Klimas et al.*, 1992; *Goertz et al.*, 1993; *Klimas et al.*, 1994], and through artificial intelligence [*Bargatze et al.*, 1985; *Hernandez et al.*, 1993; *Vassiliadis et al.*, 1995; *Gleisner and Lundstedt*, 1997; *Gavrishchaka and Ganguli*, 2001; *Gleisner and Lundstedt*, 2001; *Weigel et al.*, 2003; *Chen and Sharma*, 2006]. These models have been summarized and compared by *Li et al.* [2007]. Motivated by the good performance of a model using solar wind parameters to predict the *Dst* index [*Temerin and Li*, 2002, 2006], *Li et al.* [2007] developed two models, one simple and one more complex, to predict the *AL* index using solar wind parameters based on a combination of empirical functions similar to the *Dst* model. They obtained a prediction efficiency (PE, defined as PE = 1–(mean-squared residual)/(variance of data)) of 0.723, a linear correlation coefficient (LC) of 0.850, and a root-mean-square (RMS) error of 87.9 nT for the 10 min averaged *AL* index for the year 1995. They demonstrated that the average effects of substorms as measured by the *AL* index, though not short timescales, can be well predicted.

[1]Center for Space Science and Applied Research, Chinese Academy of Sciences, Beijing, China.
[2]Laboratory for Atmospheric and Space Physics, University of Colorado Boulder, Boulder, Colorado, USA.
[3]University of California, Berkeley, California, USA.

Corresponding author: B. Luo, Center for Space Science and Applied Research, Chinese Academy of Sciences, No. 1 Nanertiao, Zhongguancun, Haidian District, Beijing 100190, China. (luobx@nssc.ac.cn)

©2013. American Geophysical Union. All Rights Reserved.
2169-9380/13/10.1002/2013JA019188

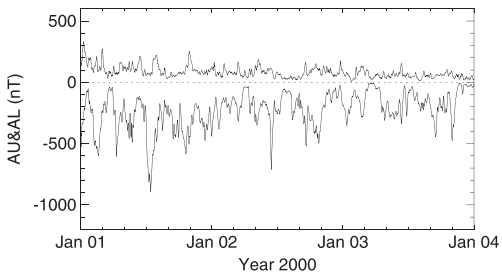

Figure 1. Comparison between the 10 min averaged *AU* and *AL* indices for days 1–3 January 2000.

[5] It is well known that the *AU* and *AL* indices behave similarly in some respects. Figure 1 shows an example of the correlation between the *AU* and the *AL* indices. The figure shows that the indices respond similarly often but not always. Around the middle of 2 January, the amplitude of *AL* increased but the *AU* decreased. Figure 2 shows the correlation between the 10 min averaged *AU* and *AL* indices for the year 1995. Their LC is –0.70. Also, the amplitude of *AU* is about 0.53 of *AL*. For the seven years, 1995–2001, the LC of *AU* and *AL* is –0.65, and the amplitude of *AU* is about 0.62 of *AL*.

[6] Since *AU* and *AL* are both auroral activity indices and somewhat correlated, we decided to develop an *AU* model to explore the differences and similarities between *AU* and *AL*. Since more provisional auroral indices and solar wind data are available than when the *AL* model was developed, we have also updated and improved the *AL* complex model developed by *Li et al.* [2007] and combined this improved *AL* model to predict the *AE* index.

2. Data

[7] The models were developed using 7 years of data. The solar wind data are from the Wind spacecraft [*Lin et al.*, 1995; *Lepping et al.*, 1995] and from the ACE spacecraft [*Smith et al.*, 1998; *McComas et al.*, 1998] after its launch in 1998 to fill gaps in the Wind data. Since 2000, we used data exclusively from ACE. All solar wind data were propagated to the magnetosphere ($t = t_{sw} - x/V_x$ where x is the upstream component of solar wind location and V_x is the magnitude of the x component of the solar wind velocity at t_{sw}) and rotated into the GSM coordinate system and interpolated to a constant 10 min interval.

[8] The provisional *AU*, *AL*, and *AE* indices are from the World Data Center (WDC) (Geomagnetism, University of Kyoto). All auroral electrojet indices have also been averaged to a 10 min interval.

3. Model Description

[9] In this study we first developed an *AU* model based on the functions used in the *AL* complex model [*Li et al.*, 2007] and then, by analyzing the characteristics of the residual and upstream solar wind parameters, we added new terms and revised the model to reduce the residual. Eventually we obtained the *AU* model. Then, based on the new terms in the *AU* model, we updated the *AL* complex model of *Li et al.* [2007] and using $AE = AU - AL$, we modeled the *AE* index. An example of the model outputs for *AU*, *AL*, and *AE*, as well as the driving solar wind parameters for a high-speed stream due to a coronal hole is shown in Figure 3. In comparing the model indices with the measured indices, there is an additional parameter that is optimized, which is the time shift between the model output and the index. For the *AU* model, the time delay added to the model output is 3.5 min, while for *AL* it is 1.5 min. In predicting the *AE* index, the modeled *AL* was interpolated to the times of *AU*. Below, we introduce the *AU* model functions. The updated *AL* model is shown in Appendix A.

[10] The output of the final *AU* model is the sum of five terms *au*1, *au*2, *P*_term, *D*_term, and *offset* (equation (1)) whose amplitudes are modulated by annual, diurnal, and semidiurnal variations (equations (2), (3), (4), (5), and (6) where $fy = 2\pi/365.24$ and t is in days since the beginning of 1995).

$$AU(t) = au1^*(t) + au2^*(t) + P_\mathrm{term}^*(t) + D_\mathrm{term}^*(t) + \mathrm{offset}^*(t), \quad (1)$$

$$\begin{aligned} au1^*(t) = {} & au1(t) \cdot (1 + 0.437 \sin(fy \cdot t + 4.97)) \\ & \cdot (1 + 0.120 \sin(4\pi \cdot t + 3.61)) \\ & \cdot [1 + 0.062 \sin(2\pi \cdot t + 3.13) \cdot (1 + 2.02 \sin(fy \cdot t + 1.27))], \end{aligned} \quad (2)$$

$$\begin{aligned} au2^*(t) = {} & au2(t) \cdot (1 + 0.28 \sin(fy \cdot t + 3.09)) \\ & \cdot (1 + 0.249 \sin(4\pi \cdot t + 5.33)) \\ & \cdot [1 + 0.070 \sin(2\pi \cdot t + 3.65) \cdot (1 + 2.34 \sin(fy \cdot t + 3.19))], \end{aligned} \quad (3)$$

$$\begin{aligned} P_\mathrm{term}^*(t) = {} & P_\mathrm{term}(t) \cdot (1 + 0.04 \sin(fy \cdot t + 5.56)) \\ & \cdot (1 + 0.17 \sin(4\pi \cdot t + 1.32)) \\ & \cdot [1 + 0.42 \sin(2\pi \cdot t + 0.18) \\ & \cdot (1 + 0.31 \sin(fy \cdot t + 0.71))], \end{aligned} \quad (4)$$

$$\begin{aligned} D_\mathrm{term}^*(t) = {} & D_\mathrm{term}(t) \cdot (1 + 0.16 \sin(fy \cdot t + 2.19)) \\ & \cdot (1 + 0.23 \sin(4\pi \cdot t + 3.28)) \\ & \cdot [1 + 0.26 \sin(2\pi \cdot t + 0.43) \\ & \cdot (1 + 2.66 \sin(fy \cdot t + 4.74))], \end{aligned} \quad (5)$$

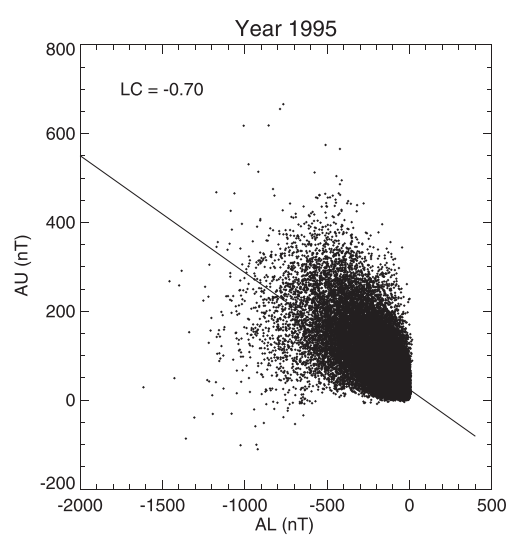

Figure 2. Correlation of the *AU* and *AL* indices for the year 1995.

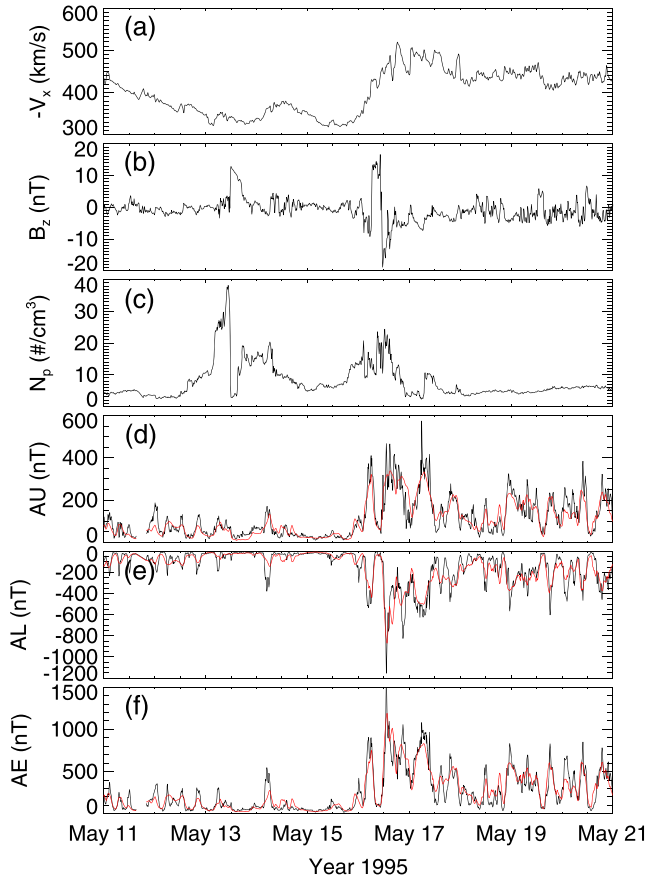

Figure 3. Relevant solar wind parameters and a comparison between the 10 min averaged measured (black) and the predicted *AU*, *AL*, and *AE* indices (red) for days 11–21 May 1995.

$$\begin{aligned}\text{offset}^*(t) = \text{offset}(t) &\cdot (1 + 1.15\sin(fy \cdot t + 4.67)) \\ &\cdot (1 + 0.34\sin(4\pi \cdot t + 2.59)) \\ &\cdot [1 + 0.24\sin(2\pi \cdot t + 4.36) \\ &\cdot (1 + 0.95\sin(fy \cdot t + 0.22))]\,. \end{aligned} \tag{6}$$

We add the time modulation because both annual and universal time variations of the auroral indices have been shown to exist [e.g., *Davis and Sugiura*, 1966, *Basu*, 1975; *Berthelier*, 1976; *Ahn et al.*, 2000a, 2000b].

[11] Similar to *Li et al.* [2007], the *au*1 term is determined by forward integration, while the *au*2 term is directly calculated from solar wind V_x and B_z values (more detailed discussion later). The significant differences between the new *AU* and *AL* models and the previous *AL* complex model [*Li et al.*, 2007] are three new terms. The *P*_term is a pressure term like the one used in *Temerin and Li* [2002, 2006] to model *Dst*. The *D*_term, which is also calculated directly from the solar wind V_x and B_z, has an opposite contribution to the modeled *AU* and *AL* compared with the *au*2 term. The reason we introduce the *D*_term is that often, *AU* decreases to a low level during the main phase of major geomagnetic storms. This will be further described later. The *offset* term, which is calculated from the $F_{10.7}$ index, replaces the formerly used offset constant (–9.868 for the complex model) in *Li et al.* [2007]. Furthermore, the driving terms of *au*1 and *al*1 are also modulated by the $F_{10.7}$ index.

[12] Similar to the *AL* complex model in *Li et al.* [2007], the *au*1 and *au*2 terms contribute most to the magnitude of the modeled *AU*, especially *au*1 is the most significant term in the *AU* model and has the largest amplitude among the five terms.

[13] The annual phases of $au1^*$ and $au2^*$, as given by equations (2) and (3), are 4.97 and 3.09, respectively. Since *au*1 and *au*2 have additional annual and diurnal variations, as do the other terms, to investigate the overall annual variation of the *AU*, *AL*, and *AE* model indices, we ran the model for artificial solar wind data. We set the density to a constant 4 cm^{-3}, B_y and B_x to zero, the solar wind velocity to a constant 450 km/s and alternated B_z so that it was +5 nT for 30 min and then –5 nT for 30 min of every hour for a whole year. The annual variation was found by averaging for *AU*, *AL*, and *AE* every day and are shown in Figures 4a, 4b, and 4c. It can be seen that the modeled *AU* shows annual variability with a maximum during the summer months and a minimum during the winter months. This variability can be associated with the winter-summer asymmetry: a higher ionospheric conductivity during the summer months drives larger ionospheric currents [*Lyatsky et al.*, 2001; *Pulkkinen et al.*, 2011]. Figures 4b and 4c show the annual variations of the *AL* and *AE* indices. The annual variation of the *AL* index shows two peaks near the equinoxes. The modeled *AE* shows a higher magnitude in summer than winter. For *AU* the higher overall ionospheric conductivity near the summer solstice dominates the annual variation, while for *AL*, the equinoctial effect, which produces stronger magnetic activity near the equinoxes, dominates the annual variation, though both indices have larger magnitudes near the summer solstice than the winter solstice.

[14] Using the outputs for the artificial solar wind data introduced above, the diurnal variation of the *AU*, *AL*, and *AE* indices was also investigated by averaging each hour for four different days (21 March, 21 June, 21 September, and 21 December) for the different seasons. The diurnal variations are shown in Figures 4d, 4e, and 4f, respectively. The average of the diurnal variations of the four seasons approximates the diurnal variation for the whole year. The *AU* index has two peaks, around 07 UT and 18 UT, while the *AL* index has a single maximum around 16 UT. The overall universal time variation of *AU* and *AL* gives a maximum around 17 UT for the *AE* index. These modeled results are consistent with the findings of *Ahn et al.* [2000b, Plate 1], who investigated the universal time variations of the auroral electrojet indices based on 20 years of data. Both the results there and in this work demonstrate clearly that the auroral electrojets are dependent upon universal time.

3.1. The *au*1 Term

[15] The functions used to calculate *au*1 are almost the same as that for the *AL* complex model in *Li et al.* [2007], but with the driving terms modulated by the $F_{10.7}$ index. First, we calculate *au*1 as

$$\begin{aligned} au1(t + \mathrm{d}t) = au1(t) + \{&-8.79 \cdot (au1(t))^{1.289} \\ &\cdot (1 + 0.00092au1(t - 0.0556)) \\ &+ \mathrm{d}f2(t) \cdot |(1 - 0.00067au1(t - 0.0556)) \\ &\cdot (1 + 0.00171au1(t - 0.0556))| \\ &\cdot [1 - \mathrm{erf}(0.046\,(B_z(t) + 0.37\,|B_z(t)|))]\} \cdot \mathrm{d}t, \end{aligned} \tag{7}$$

and *au*1 is set to zero should it ever be less than zero.

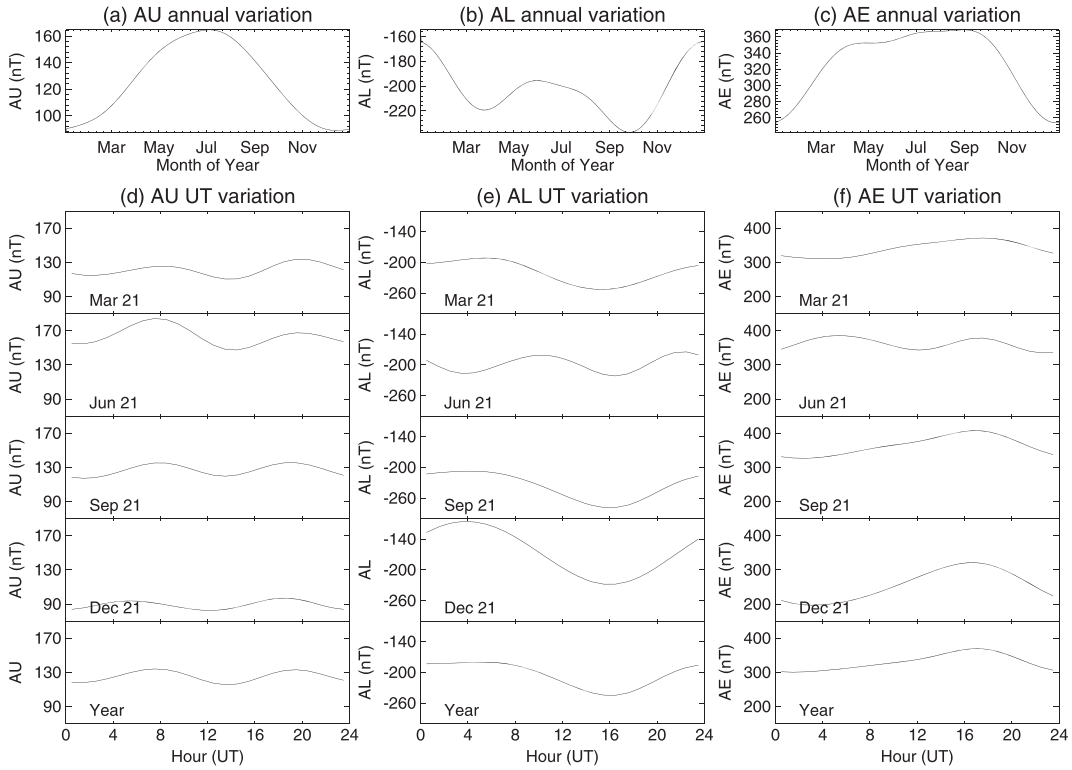

Figure 4. The annual and universal time (UT) variations given by the models for the *AU*, *AL*, and *AE* indices using artificial solar wind parameters as input (see text). (a) Annual variation for the *AU* index; (b) Annual variation for the *AL* index; (c) Annual variation for the *AE* index; (d) UT variation for the *AU* index; (e) UT variation for the *AL* index; (f) UT variation for the *AE* index.

[16] The right hand of equation (7) includes three parts, $au1(t)$ for the previous time step, $-8.79 \cdot (au1(t))^{1.289}$ for the decay, and $df2(t)$ which is the driving term for growth.

[17] For the parameters of the decay term, for $au1$ = 100 nT and 300 nT, the decay timescale is about 0.72 h and 0.52 h, respectively.

[18] The $df2(t)$ term is calculated by equation (8), which is a function of $\sin\phi$ which is nominally the sine of the angle between the magnetic dipole axis and the Sun-Earth line ($\sin\phi = \sqrt{1-\cos^2\phi}$ where $\cos\phi$ is calculated by equation (9)) [*Li et al.*, 2007; *Temerin and Li*, 2002, 2006] and $fe2(t)$ which is directly determined by the solar wind parameters through equations (10) and (11) and modulated by the $F_{10.7}$ index. For the *AU* model, the optimized revolution angle of the Earth around the Sun, the rotation angle of the Earth, and the magnitude of the offset of the dipole axis from the rotation axis are –0.255 radians, –1.58 radians, and 0.058 radians (reflected by the value 0.0531 and 0.0579), respectively. The $(\sin\phi(t))^{2.00}$ factor provides for the equinoctial effect, maximum near the equinoxes and minimum at the solstices, for the $au1$ term. The main difference between $df2(t)$ term here and the one used in the former *AL* complex model is in the $F_{10.7}$ modulation. It was set as free parameter, and its value was determined by minimizing the RMS error of the model. As an ultraviolet (UV) flux proxy, $F_{10.7}$ reflects the conductivity of the ionosphere through ionization. This can influence the intensity of the auroral electrojets. According to equation (8), a larger $F_{10.7}$ increases the driving term and thus produces a more intense eastward electrojet. We use the daily measured $F_{10.7}$ interpolated to the 10 min intervals. The $df2$ has a maximum of 6081 if we neglect the modulation of $F_{10.7}$ because $fe2$ is always negative based on (10) and (11) and thus the $df2 \cdot dt$ in equation (7) will not exceed 42.2 nT per a 10 min time step. For an $F_{10.7}$ index of 100 sfu and 200 sfu, this number increases to 49.8 and 57.2, respectively. For *AL*, however, the driving term decreases with increasing $F_{10.7}$. This is one of the more interesting results of our study and is discussed further later.

$$df2(t) = -6081 \cdot \left(1.0 + 1.775 \times 10^{-3} \cdot F_{10.7}\right) \cdot (\sin\phi(t))^{2.00} \cdot fe2(t) \big/ (1.0 - fe2(t)) \tag{8}$$

$$\cos\phi = \sin(fy \cdot t - 0.255) \cdot 0.0531 \cdot \sin(2\pi \cdot t - fy \cdot t - 1.58) + \cos(fy \cdot t - 0.255) \cdot (0.39 + 0.0579 \cdot \cos(2\pi \cdot t - fy \cdot t - 1.58)) \tag{9}$$

$$fe2(t) = fe1(t) + (fe1(t - 0.0486) - fe1(t)) \cdot 0.121 \tag{10}$$

$$fe1(t) = -9.01 \times 10^{-2} \cdot (B_t(t))^{1.996} \cdot (\sin\theta(t))^{7.63} \cdot (V_x(t)/430)^{3.52} \cdot \left(N_p(t)/7\right)^{0.39} \cdot \left[1 + \mathrm{erf}\left(0.0341 \cdot dh(t) \cdot B_p(t) \cdot \cos(\mathrm{ang}(t) + 5.27)\right)\right] \tag{11}$$

[19] According to equation (11), where B_p is the magnitude of the interplanetary magnetic field (IMF) in nT in the GSM x–y plane, B_t is the magnitude of IMF in the plane perpendicular to the Sun-Earth line and $\theta = -(\arccos(-B_z/B_t) - \pi)/2$ where B_z is the z component of the IMF in GSM

coordinates, V_x is the x component of solar wind velocity, N_p is the solar wind density in cm^{-3}, the magnitude of $fe1$ is directly calculated from solar wind parameters. The power of each solar wind parameter reflects the relative significance of this solar wind parameter in determining the magnitude of $fe1$ and thus the growth of the *AU* index. It can be seen that solar wind speed and interplanetary magnetic field play a dominant role while the solar wind density plays a smaller role. These features have been verified by previous work that studied the relationship between solar wind parameters and geomagnetic indices [e.g., *Temerin and Li*, 2002, 2006; *Li et al.*, 2007; *Newell et al.*, 2008] that have a critical relationship with substorms and high-energy electrons in the plasma sheet and radiation belts [e.g., *Luo et al.*, 2011; *Li et al.*, 2011]. The parameters ang(t) and dh(t) are given by equations (12) and (13), respectively.

$$\mathrm{ang}(t) = \arctan\left(B_x(t), B_y(t)\right), \tag{12}$$

$$\mathrm{d}h(t) = -0.99 \cdot \cos(fy \cdot t - 1.54) + \sin(2\pi \cdot t - 0.36), \tag{13}$$

[20] The physical interpretation of the $au1$ term is that the solar wind through reconnection drives the intensity of the auroral electrojets. The auroral electrojets then decay when the driver becomes less efficient or is removed. The form of the driver term then represents the efficiency of the solar wind in driving the auroral electrojets together with the effect of ionospheric conductivity by including the $F_{10.7}$ index.

3.2. The *au*2 Term

[21] The $au2$ term is calculated directly from the solar wind velocity V_x and IMF B_z. It is modulated by the $\sin\phi$ term and thus has an equinoctial variation (equation (14)). By optimizing the model parameters, the $au2$ term is determined by V_x and B_z 70 min (i.e., at time $(t - 0.0486)$) before. Equation (15) provides that if $au2'$ is negative, $au2'$ will be set zero. Thus, the $au2$ term only has positive values and will intensify the *AU* index during negative IMF B_z periods. Equation (16) provides for smoothing. In equation (16) $\mathrm{smooth}^{50}(au2''(t), 3)$ means that the three-point running average is applied 50 times. When doing the smoothing for each point at t_0, the "future" points of $au2''$ starting after $t_0 + 0.0486$, which should be unknown in a real-time prediction, have been set to the $au2''$ values of points before time $t_0 - 0.0486$ symmetrically. Such handling will be adopted as well for other smoothings in the *AU* and *AL* models. The $au2$ term is much smaller than the $au1$ term. However, the fact that the addition of this term improves the model shows that there is something missing in the $au1$ term. We do not have a good physical interpretation of what that may be.

$$au2'(t) = -3.29 \cdot B_z(t - 0.0486) \cdot (V_x(t - 0.0486)/430)^{1.10} \cdot (\sin\phi(t - 0.0486))^{-6.73} \tag{14}$$

$$au2''(t) = au2'(t) + |au2'(t)| \tag{15}$$

$$au2(t) = \mathrm{smooth}^{50}\left(au2''(t), 3\right) \tag{16}$$

3.3. *P*_term

[22] The P_term is similar to the pressure term in the *Dst* models [*Temerin and Li*, 2002, 2006], and for the *AU* model, it has relevant parameters as shown in equation (17). The pressure term is understood to be due to magnetopause currents and produces only a small contribution to *AU* and *AL*.

$$P_\mathrm{term}(t) = \left\{-0.77 \cdot (B_t(t))^2 \cdot \left(1 - 0.09 \cdot N_p(t)\right) + \left[4.80 \times 10^{-4} \cdot (\sin\phi(t))^{0.81} \cdot (V_x(t))^2 - 30.5\right] \cdot N_p(t)\right\}^{0.5} \tag{17}$$

3.4. *D*_term

[23] The D_term is also calculated from the solar wind velocity V_x and IMF B_z, but has an opposite contribution to the *AU* index compared with the $au2$ term. The D_term only has a finite value when V_x and IMF B_z exceed a threshold. The reason the D_term is introduced is that during the main phase of major storms, when the solar wind speed is high and accompanied by a long lasting southward B_z, *AU* often drops to a low level. For these events, $au1$ and $au2$ would have rather high values and thus the magnitude of the predicted *AU* index would be very large, causing large errors during major geomagnetic storms. The drop in *AU* during large magnetic storms may happen because the current system responsible for *AU* moves equatorward of the auroral zone magnetometers that measure *AU*. Considering that during the main phase of major geomagnetic storms, the solar wind speed is high and IMF B_z is southward, we use a term similar to the smoothed V_xB_z with a certain time lag to correct the model, as shown by equations (18), (19), and (20). From equations (18) and (19), the D_term is determined by eight times smoothed $(V_x/500)^{0.86}B_z$ about 30 min (i.e., $(t - 0.0208)$) before. Equation (19) provides a threshold for the D_term'' of –7.3. That is, if the D_term'' is greater than –7.3, the D_term will be set to zero and there will be no correction in the *AU* model.

$$D_\mathrm{term}'(t) = 0.50 \cdot (B_z(t - 0.0208) - |B_z(t - 0.0208)|) \cdot (V_x(t - 0.0208)/500)^{0.86} \tag{18}$$

$$D_\mathrm{term}''(t) = \mathrm{smooth}^8\left(D_\mathrm{term}'(t), 3\right) < -7.3 \tag{19}$$

$$D_\mathrm{term}(t) = \left[47.6 + 17.8 \cdot D_\mathrm{term}''(t)\right](\sin\phi(t))^{2.92} \tag{20}$$

[24] An example of the quick drop of the *AU* index is shown in Figure 5b. Also shown are the modeled *AU* and the contributions of the five terms to the *AU* model. Just before 7 April, a major geomagnetic storm occurred. As the magnitude of the D_{st} index increased, the magnitude of the *AU* index gradually decreased. The positive $au1$ and $au2$ components both increase significantly, while the magnitude of the negative D_term increases, too. The overall effect is that, the three terms cancel each other and the final modeled *AU* shows good agreement with the measured *AU* index.

3.5. The *offset* Term

[25] In the early development of the *AU* model, the *offset* was a constant as it was in the *AL* model in *Li et al.* [2007]. When we compared the modeled and measured *AU* year by year from 1995 to 2001, we found that the yearly residual had a rather high correlation (correlation coefficient = 0.71) with the yearly solar radio flux $F_{10.7}$. So in the *AU* model, the constant offset was replaced by an *offset* term that is calculated from $F_{10.7}$. The monthly and yearly averaged *offset* for the *AU* and the *AL* models from 1995 to 2001, together

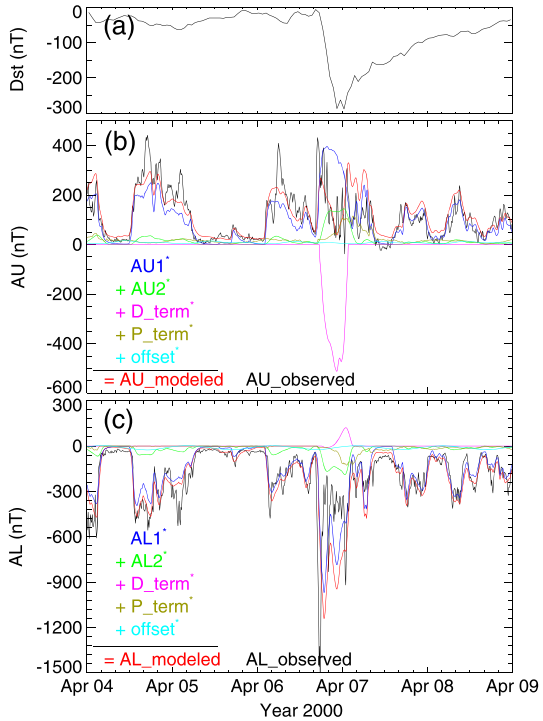

Figure 5. The modeled *AU* (same for the *AL*) is the sum of five terms, *au*1, *au*2, *P*_term, *D*_term, and *offset*, as indicated by equation (1). (a) *Dst* index; (b) an example of *AU* (red), *au*1 (blue), *au*2 (green), *D*_term (purple), *P*_term (yellow), *offset* (sky blue), and the measured *AU* (black) for days 4–9 April 2000 when a major geomagnetic storm occurred as shown by the *Dst* index in Figure 5a. (c) the prediction of the *AL* for the same period.

with the monthly and yearly averaged $F_{10.7}$, are shown in Figure 6. $F_{10.7}$ is a proxy for solar ultraviolet flux, which in turn changes the conductivity of the ionosphere through ionization. So one would expect the offset to change with the solar cycle. The solar cycle variation of the auroral electrojet indices have been investigated [*Ahn et al.*, 2000b]. Furthermore, the offset is modulated by the annual and diurnal variations in equation (6).

[26] The *offset* term, which now is related to $F_{10.7}$, further reflects the effects of solar UV intensity and thus the conductivity of the ionosphere on auroral activity. One might have expected that the effects of $F_{10.7}$ would have been captured completely by the $F_{10.7}$ modulation of the driver term *au*1. That they are not shows that $F_{10.7}$ has a relatively greater contribution during low levels of magnetospheric activity. This is perhaps because during higher levels of magnetospheric activity, auroral precipitation can be the main cause of ionospheric ionization and thus UV ionization as indicated by $F_{10.7}$ is relatively less important.

$$\text{offset} = (0.0613 \cdot F_{10.7} - 4.08) \cdot (\sin\phi(t))^{-5.03} \qquad (21)$$

4. Results and Discussion

[27] Parameters of both of the *AU* and updated *AL* models were found by minimizing the RMS error between the model and the measured indices, based on the solar wind data and provisional auroral electrojet indices for the years 1995–2001, the minimum of solar cycle 22 and inclining phase and maximum of solar cycle 23. The root square minimization was done "by hand." That is, we ran a program that calculated the auroral electrojet indices and the RMS error using the measured solar wind and $F_{10.7}$ values. We then changed parameters in the program and calculated a new RMS error and so forth. We also often tried different functional forms by starting with formulations similar to *Li et al.* [2007]. After a few months of work, we came up with the present results. Compared with the former *AL* model developed in *Li et al.* [2007], much more data have been used to develop the *AU* and new *AL* models. In addition, $F_{10.7}$ modulation of the driving term and three new terms including the solar wind pressure, sudden drops of the indices during the main phases of the major storms, and an *offset* term related to the progress of the solar cycle were added.

4.1. Overall Results of the Modeled *AU*, *AL*, and the *AE* Indices for 1995–2001

[28] For the seven years, 1995–2001, the *AU* model gives a prediction efficiency (PE) of 0.716, an LC of 0.846, and an RMS error of 39.3 nT, while the updated *AL* model gives a PE of 0.715, a linear correlation coefficient of 0.846, and an RMS error of 81.6 nT. Based on the predicted *AU* and *AL*, we can predict *AE* with a PE of 0.788, an LC of 0.888, and an RMS error of 95.7 nT.

[29] It is evident that the PE and LC for the *AE* index are larger than for the *AU* and the *AL* indices individually. To investigate the reason, we calculated the LC for the modeled *AU* and *AL* indices, which is shown in Figure 7a. The correlation coefficient for the residuals of the *AU* model and the *AL* model was also calculated and shown in Figure 7b. We can see that the modeled *AU* and *AL* indices are correlated,

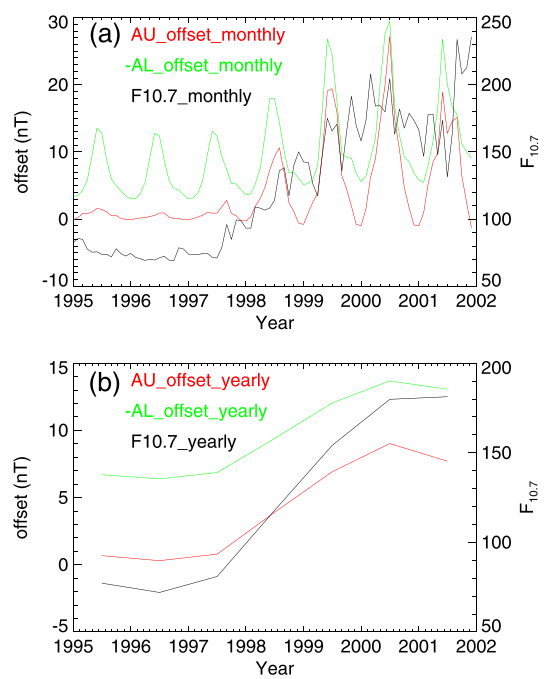

Figure 6. The (a) monthly and (b) yearly averages of *offset* term of the *AU* (red line) and *AL* (green line) models for years 1995–2001, in comparison with the monthly and yearly averages of $F_{10.7}$ index (black line).

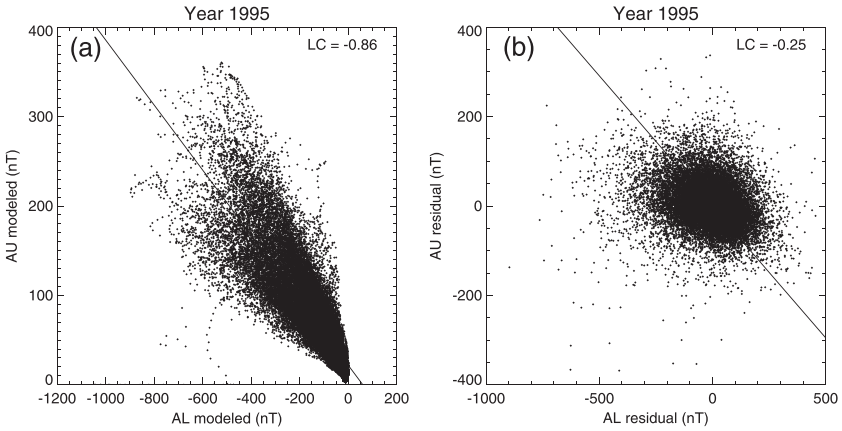

Figure 7. (a) Correlation of the modeled *AU* and *AL* indices for the year 1995; (b) Correlation of residuals of the modeled *AU* and *AL* indices for the year 1995.

though with an LC of –0.86, the correlation is larger in magnitude than the –0.70 for the observed indices for the year 1995. The LC for the residuals of the models is significantly lower with a value of –0.25. For the years 1995–2001, the LC of predicted *AU* and *AL* is –0.82, while the LC of their residuals is –0.20. Thus, in calculating *AE* using the modeled *AU* and *AL* by $AE = AU - AL$, the signal represented by *AU* and *AL* adds coherently, while the error adds incoherently.

[30] One of the features of the *AL* model of *Li et al.* [2007] was that the model predicted a smoothed version of *AL* better than the 10 min version even though optimized to predict the 10 min version. The *AU* and updated *AL* models are similar. The models have the best prediction efficiency when compared with the 13-point (2 h, 10 min) running average of the auroral electrojet indices for which the *AU* model has a PE of 0.795, an RMS error of 30.4 nT, and an LC of 0.893, while the updated *AL* model has a PE of 0.806, an RMS error of 59.2 nT, and an LC of 0.900. For the *AE* index, the numbers are 0.850, 73.5 nT, and 0.923. The PE is even better when the 13-point running average of the model results are compared with the 13-point running average of the indices: PE of 0.814, RMS error of 29.0 nT, and LC of 0.902 for *AU*, while PE of 0.837, RMS error of 54.3 nT, and LC of 0.915 for *AL*. The numbers for the *AE* index are 0.874, 67.1 nT, and

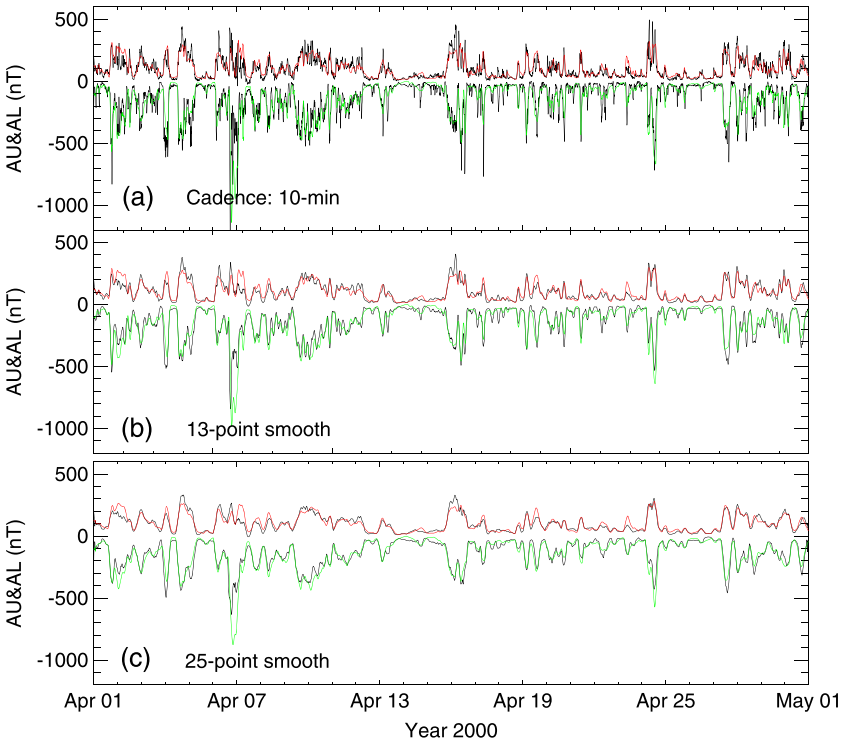

Figure 8. Comparison of the modeled *AU* (red) and *AL* (green) with the measured *AU* and *AL* (black) indices. (a) Modeled *AU* and *AL* (10 min resolution) and 10 min averaged *AU* and *AL* indices; comparisons of the (b) 13-point and (c) 25-point running average of the modeled and measured 10 min averaged *AU* and *AL* indices.

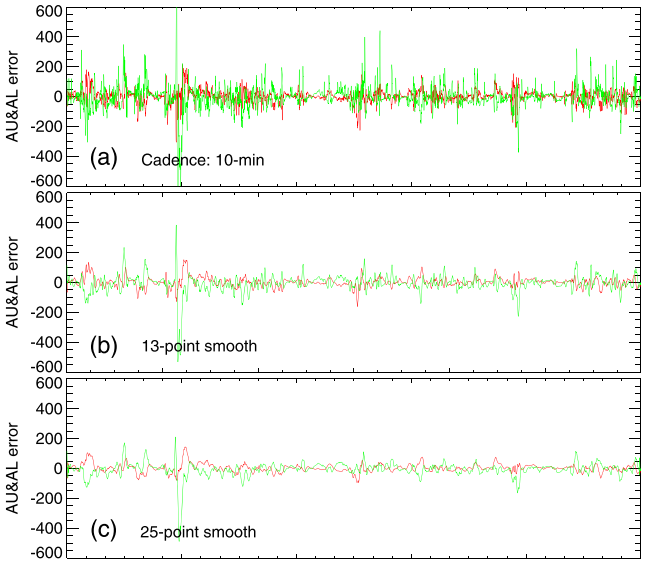

Figure 9. Differences between the modeled and the measured *AU* (red) and *AL* (green) indices. (a) Differences for modeled *AU* and *AL* (10 min resolution) and 10 min averaged *AU* and *AL* indices; differences for the (b) 13-point and (c) 25-point running average of the modeled and measured 10 min averaged *AU* and *AL* indices.

0.935. For the 25-point running average of both the model and the auroral electrojet indices, the *AU* model gets a PE of 0.851, an RMS error of 24.4 nT, and an LC of 0.923 while the *AL* model gets a PE of 0.881, an RMS error of 42.6 nT, and an LC of 0.939. The numbers for the *AE* index are 0.907, 53.8 nT, 0.952. Figure 8 shows the prediction compared with the measured *AU* and *AL* indices when the smoothing number is changed. Figure 9 shows the differences between the modeled and measured *AU* and *AL* indices. It can be seen that both *AU* and *AL* models predict the longer time averaged index well, but predict shorter timescale variations poorly.

4.2. Improvements by Adding New Terms to the Model

[31] As has been discussed, the main difference of the *AU* model and updated *AL* model from the former *AL* complex model in *Li et al.* [2007] is that three new terms were added together with the additional modulation of the driver term by $F_{10.7}$. It is a natural question to ask how each of these terms improves the model. In Table 1, the performance of the model for different combinations of terms is listed. It can be seen that for the *AU* model, the *D*_term improves the model significantly, while the *P*_term and *offset* improve the model to a lesser degree. The *D*_term takes effect during major geomagnetic storms and has a much larger magnitude. If no *D*_term is included, the errors of the model would be very large during major geomagnetic storms and make the performance of the model much poorer. The pressure term shows that the solar wind dynamic pressure also affects the auroral electrojet indices. Also, in addition to the *offset* term, there is an $F_{10.7}$ modulation of the driver term *au*1. The $F_{10.7}$ index is a proxy for ultraviolet intensity and reflects the conductivity of the ionosphere. This shows that solar UV intensity plays a significant role in auroral activity.

[32] Compared with the *AU* model, the improvement to the *AL* model using the three new terms is smaller. Figure 5 shows the prediction of the *AU* and *AL* compared with the measured values for days 4–9 April 2000. During the first half of this period, the geomagnetic field showed minor disturbance, while on the second half of this period, a major geomagnetic storm occurred. It can be seen that before and around the peak of the geomagnetic storm, the magnitude of both *AU* and *AL* decreased. Including the new term *D*_term improves the performance of the prediction. By comparing the magnitudes of *D*_term for *AU* and *AL*, it can be seen that the *D*_term with a magnitude of about 500 nT for *AU* is larger than that of about 150 nT for *AL*. Considering that, on average, the magnitude of *AL* is usually bigger than *AU*, this means that, on average, the relative magnitude of *AL* does not drop nearly as much as *AU* during major storms. The different behavior of *AU* and *AL* during major geomagnetic storms is probably due to the current systems responsible for *AU* and *AL*. *Xu* [2009] has shown that the eastward current system responsible for *AU* moves equatorward with increasing activity, but the westward current system responsible for *AL* does not. This means that, for increasing activity, the current responsible for *AU* may move equatorward of the AE magnetometers. The eastward electrojet responsible for *AU* occurs in the afternoon and dusk sectors of the auroral oval and moves equatorward with the expanding auroral oval during large magnetic storms. The westward electrojet responsible for *AL* occurs in the midnight and dusk sectors. Near midnight, during major storms, a poleward surge of the aurora keeps the westward electrojet over the AE magnetometers.

Table 1. A Summary of *AU* and *AL* Model Results for 1995–2001

		1995–2001			1995		
Model	Included Terms	PE	LC[a]	RMS[b] (nT)	PE	LC[a]	RMS[b] (nT)
AU	au1+au2+offset_const[c]	0.638	0.801	44.4	0.664	0.815	39.0
	au1+au2+offset_term[d]	0.644	0.806	44.0	0.663	0.815	39.0
	au1+au2+offset_term+*P*_term	0.652	0.814	43.5	0.682	0.827	37.9
	au1+au2+offset_term+*P*_term+*D*_term	0.716	0.846	39.3	0.700	0.837	36.8
AL	al1+al2+offset_const[c]	0.707	0.841	82.8	0.713	0.845	88.9
	al1+al2+offset_term[d]	0.709	0.842	82.4	0.712	0.845	89.1
	al1+al2+offset_term+*P*_term	0.713	0.845	81.9	0.720	0.849	87.9
	al1+al2+offset_term+*P*_term+*D*_term	0.715	0.846	81.6	0.720	0.849	87.9

[a]LC refers to the linear correlation coefficient between the modeled and observed index.
[b]RMS refers to the RMS error of the model prediction.
[c]The offset is a constant as in the previous *AL* model introduced in *Li et al.* [2007].
[d]The offset is a term related to $F_{10.7}$ which is described in this paper.

Table 2. Out of Sample Comparison for the Years 2002–2007 of the *AU*, *AL*, and *AE* Prediction

	AU			AL			AE		
Year	LC	PE	RMS (nT)	LC	PE	RMS (nT)	LC	PE	RMS (nT)
2002	0.843	0.710	44.5	0.838	0.702	83.8	0.883	0.780	102.5
2003	0.787	0.576	58.7	0.790	0.622	125.5	0.837	0.689	149.0
2004	0.751	0.551	47.7	0.828	0.684	102.0	0.855	0.731	117.8
2005	0.837	0.698	41.4	0.829	0.686	93.5	0.877	0.768	107.5
2006	0.820	0.664	33.6	0.841	0.706	74.6	0.880	0.771	86.0
2007	0.821	0.643	30.2	0.820	0.648	71.0	0.862	0.712	84.4
2002–2007	0.823	0.676	43.7	0.829	0.687	93.5	0.871	0.758	110.0

[33] From Table 1, it can be seen that the RMS error of the *AU* model is larger for 1995–2001 than for 1995, while the RMS error of the *AL* model is smaller for 1995–2001 than for 1995. This may be because the average observational *AU* is larger for 1995–2001 than for 1995 and opposite for the *AL* index.

4.3. Solar Ultraviolet Effects on *AU* and *AL*

[34] One of the more interesting results of our study is that the magnitude of *AU* increases with increasing $F_{10.7}$, but the magnitude of *AL* decreases with increasing $F_{10.7}$ for similar solar wind conditions. During the study period, 1995–2001, the $F_{10.7}$ index ranged from 64.9 sfu to 284.5 sfu. The corresponding increase in the factor modulating the main driving term for *AU* (equation (8)) is 35.0%. The corresponding decrease in the factor modulating the main driving term for *AL* is 35.7%. Needless to say, these are significant effects. How do we interpret this? While not providing a full explanation, we note that the different behavior of *AU* and *AL* is consistent with the difference in the seasonal variations of *AU* and *AL*. *AU* is more sensitive to changes in the UV ionization of the ionosphere as shown by its peak near the summer solstice, while *AL* is relatively more sensitive to magnetospheric activity. The opposite behavior of *AU* and *AL* with respect to $F_{10.7}$ could then be a consequence of decreased overall magnetospheric activity due to increased ionospheric ionization as the ionosphere produces more drag on the overall magnetospheric convection with increased ionization. *Ober et al.* [2003] have argued that the increased Pederson conductivity associated with an increased $F_{10.7}$ index decreases the polar cap potential. We would like to note that this explanation is not inconsistent with the larger *AL* magnitude near the summer solstice, as ionospheric currents would still prefer the higher conductivity of the summer ionosphere.

[35] Another and probably more important reason that the magnitude of *AL* decreases with increasing $F_{10.7}$ is that the auroral acceleration region moves up in altitude with increasing $F_{10.7}$ as shown by *Cattell et al.* [2013] presumably due to the increased scale height of the ionosphere in response to increased solar ultraviolet radiation. When the acceleration region is higher, smaller potentials along magnetic field lines are needed to carry the same field-aligned current. A smaller auroral potential means less energy deposited into the ionosphere and less ionization by auroral electrons. Less ionization means a smaller electrical conductivity. A smaller conductivity means a smaller ionospheric hall current and thus smaller *AL*. This is not so important for *AU* since the eastward electrojet responsible for *AU* occurs in the afternoon and dusk sectors where ionization by auroral precipitation is relatively less important. The increase in *AU* with $F_{10.7}$ is interpreted as due to an increase in ionospheric conductivity and thus ionospheric currents.

4.4. Out of Sample Comparison for Years 2002–2007

[36] Since the provisional auroral electrojet indices are available for years 2002–2007, we have used these years to test the *AU* and updated *AL* models. The *AU* model gave a PE of 0.676, an RMS error of 43.7 nT, and an LC of 0.823. The updated *AL* model gave a PE of 0.687, an RMS error of 93.5 nT, and an LC of 0.829. The *AE* prediction gives a PE of 0.758, an RMS error of 110.0 nT, and an LC of 0.871. We also examined the model's prediction for each year separately. The results are summarized in Table 2. It can be seen that the overall prediction performance is good, though with a little smaller PE and LC than for the years 1995–2001. Looking at the individual years in Table 2, it is seen that the correlation between the model and measured auroral electrojet indices are good except for the years 2003 and 2004. We examined the prediction in these two years and found that large errors were caused by very large geomagnetic storms. For year 2004, if we exclude the time period of only one major geomagnetic storm, the PE of the *AU* model would goes up to 0.60. This means that although we have adopted a new term *D*_term to improve the behavior of models, the temporal fluctuations and the magnitude of the auroral electrojet indices during major storms are still hard to predict correctly.

[37] The PE for the year 2007 also shows somewhat smaller values. We inspected the provisional auroral electrojet indices data and found that for year 2007 the data are based on relatively fewer stations than for other years. Fewer reporting stations have an effect on the indices [*Takahashi et al.*, 2004]. Because *AU* and *AL* are the magnitudes of the *H* component of the magnetic field of the station with the largest positive and negative magnitude, *AU* and *AL* indices based on fewer stations will be equal to or less than the magnitude of what a 12-station *AU* and *AL* would be. The provisional *AU* and *AL* might have smaller magnitudes, and our models may over predict. Considering this, we could get a better PE by making a simple linear adjustment to the predicted indices. By multiplying the modeled *AU* and *AL* for 2007 by 0.88, we can get a PE of 0.674 and 0.681, respectively. It should also be noted that the provisional *AU* and *AL* indices for the years 1995–2001 are typically based on 10 or 11 stations rather than the official 12. This means that our model will typically underpredict a 12-station *AU* or *AL* index. In addition, the variation in the number of stations introduces an additional error.

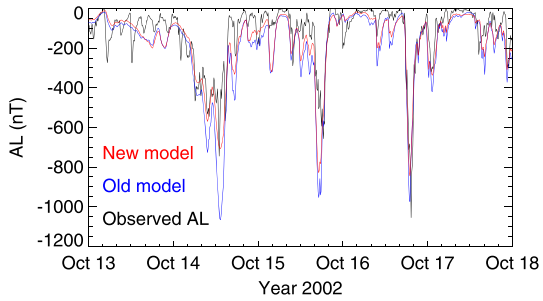

Figure 10. Predicted *AL* from both the old (blue) and updated (red) *AL* models, as well as the measured *AL* index (black) for 13–18 October 2002.

[38] The out-of-sample performance comparison of the new and old *AL* models was also done based on the 2002–2007 data. The old *AL* model gives a PE of 0.649, an LC of 0.817, and an RMS error of 99.0 nT, while the new model gives a PE of 0.687, an LC of 0.829, and an RMS error of 93.5 nT. In order to investigate what makes the most significant improvement in the new *AL* model compared with the old model, we tested the performance of the new *AL* model by gradually changing its parameters to the old *AL* model. We got the following results. By removing the three new terms in the new *AL* model, the PE degrades from 0.687 to 0.680. By further setting the parameters of the *al*1 term as the old *AL* model, the PE degrades from 0.680 to 0.668. By further setting the parameters in the *al*2 term as the old *AL* model, the PE degrades from 0.668 to 0.652. By further setting the parameters of $\sin\phi$ and smoothing times of *al*1 and *al*2, the PE degrades from 0.652 to 0.648, which is comparable to the old *AL* model. Also, the *D*_term degrades the performance of the out-of-sample test of the new *AL* model, implying that it is not a significant feature of the *AL* model, and the small improvement due to the *D*_term for the in-sample data may have been due to chance. However, for *AU* including the *D*_term substantially improves the PE, and the out-of-sample improvement is even better. The improvement of the new *AL* model comes from two aspects. One is that three new terms and the $F_{10.7}$ modulation of the driver term were added to the new model. The other is that the new model is optimized based on 7 years of data while the old model was based on 1 year of data. In Figure 10 the predicted *AL* from both the old and updated *AL* models are plotted to give a direct comparison for 13–18 October 2002.

4.5. Sources of Errors of the Models

[39] There are several sources of errors. First, there is uncertainty in the assumed propagation of the solar wind to the Earth [*Weimer et al.*, 2003; *Bargatze et al.*, 2005] by using the simple ballistic propagation scheme. But according to the very low correlation coefficient of the residuals of the *AU* and *AL* models, the error caused by the solar wind propagation method should not be significant. If the error caused by the solar wind propagation method had been large, the model errors would be more correlated.

[40] There is also error caused by the auroral indices themselves. Because they depend on the particular station that sees the largest current with respect to the auroral current system, similar auroral currents can produce dissimilar values of auroral indices depending on the relative location of that station and, as mentioned already, sometimes one or more stations are missing in the provisional AE indices.

[41] The third source of error is from the models. First, the timing and magnitude of particular substorms that affect the auroral electrojet indices have been studied by many people [*Rostoker et al.*, 1980; *Weimer*, 1994, 1995; *Kamide and Kokubun*, 1995; *Rostoker*, 2002; *Sharma et al.*, 2003]. How well the functions included in our model can interpret auroral current system is still questionable. The functions might cause the main error in the prediction. Second, the model parameters were found by minimizing the RMS error of the model results versus the provisional indices. We did a lot of smoothing to minimize the RMS error. Such smoothing means that the short timescale variations cannot be predicted well. Third, the more data used to develop the model, the more accurate the model should be. Compared with the former *AL* model in *Li et al.* [2007], the updated *AL* model showed better results because it was developed using 7 years of data while the former was based on only 1 year of data.

5. Summary and Conclusions

[42] Two empirical models, one newly developed for the *AU* index and the other updated for the *AL* complex model developed by *Li et al.* [2007], were introduced to predict the 10 min resolution auroral electrojet indices. Both of the models were developed using solar wind and $F_{10.7}$ data and provisional auroral electrojet indices for years 1995–2001. The *AE* index can also be predicted using $AE = AU - AL$. For years 1995–2001, the prediction efficiency (PE) of the *AU* model was 0.716, with a root mean square (RMS) error of 39.3 nT and a linear correlation coefficient (LC) of 0.846, while the *AL* model gave a PE of 0.715, an RMS error of 81.6 nT, and an LC of 0.846 and the *AE* prediction gave a PE of 0.788, an RMS error of 95.7 nT, and an LC of 0.888.

[43] Both models predict longer time-averaged variations of the auroral electrojets well, but the shorter timescale variations are much less predictable. The annual and universal time variations of the *AU*, *AL*, and *AE* indices are clearly demonstrated by the models, in agreement with former statistical studies. *AU* and *AE* have clear annual variations with maximum near summer and minimum near winter. The *AL* index also has peaks near the equinoxes. *AE* and *AL* indices have one maximum around 15 UT and 17 UT, respectively, while for the *AU* index, there are two peaks around 07 UT and 18 UT. The models show that the solar wind velocity and interplanetary magnetic field play a dominant role in controlling the auroral electrojet indices, while the solar wind density plays a smaller role. The solar ultraviolet flux also plays an important role in determining the growth of the auroral electrojet indices, though solar ultraviolet flux has opposite effects on the magnitude of *AU* and *AL*. Furthermore, a new term, which is added to model the sudden drop of auroral electrojet indices during major geomagnetic storms, improves the *AU* model significantly but is less important for the *AL* model. This indicates that the *AU* and *AL* indices behave differently during major geomagnetic storms.

Appendix A: Updated *AL* Model

$$AL(t) = al1^*(t) + al2^*(t) + P_\mathrm{term}^*(t) + D_\mathrm{term}^*(t) + \mathrm{offset}^*(t) \quad \text{(A1)}$$

$$al1^*(t) = al1(t) \cdot (1 + 0.139 \sin(fy \cdot t + 2.03)) \cdot (1 + 0.009 \sin(4\pi \cdot t + 3.89)) \cdot [1 + 0.125 \sin(2\pi \cdot t + 3.77) \cdot (1 + 1.32 \sin(fy \cdot t + 1.73))]. \quad \text{(A2)}$$

$$al2^*(t) = al2(t) \cdot (1 + 0.91 \sin(fy \cdot t + 4.69)) \cdot (1 + 0.353 \sin(4\pi \cdot t + 5.67)) \cdot [1 + 0.152 \sin(2\pi \cdot t + 3.82) \cdot (1 + 1.15 \sin(fy \cdot t + 2.93))]. \quad \text{(A3)}$$

$$P_\text{term}^*(t) = P_\text{term}(t) \cdot (1 + 0.54 \sin(fy \cdot t + 5.59)) \cdot (1 + 0.61 \sin(4\pi \cdot t + 1.14)) \cdot [1 + 0.42 \sin(2\pi \cdot t - 0.04) \cdot (1 + 2.03 \sin(fy \cdot t + 4.73))]. \quad \text{(A4)}$$

$$D_\text{term}^*(t) = D_\text{term}(t) \cdot (1 + 0.62 \sin(fy \cdot t + 2.55)) \cdot (1 + 0.49 \sin(4\pi \cdot t + 0.55)) \cdot [1 + 0.64 \sin(2\pi \cdot t + 0.31) \cdot (1 + 9.01 \sin(fy \cdot t + 4.92))]. \quad \text{(A5)}$$

$$\text{offset}^*(t) = \text{offset}(t) \cdot (1 + 0.61 \sin(fy \cdot t + 4.61)) \cdot (1 + 0.08 \sin(4\pi \cdot t + 4.57)) \cdot [1 + 1.05 \sin(2\pi \cdot t + 3.59) \cdot (1 + 0.75 \sin(fy \cdot t + 1.27))]. \quad \text{(A6)}$$

A1. The *al*1

$$al1(t + \mathrm{d}t) = al1(t) + \{9.26 \cdot (-al1(t))^{1.199} \cdot (1 - 0.00107 al1(t - 0.0625)) + \mathrm{d}f2(t) \cdot |(1 + 0.00072 al1(t - 0.0625)) \cdot (1 - 0.00137 al1(t - 0.0625))| \cdot [1 - \mathrm{erf}(0.042 (B_z(t - 0.0208) + 0.27 |B_z(t - 0.0208)|))]\} \cdot \mathrm{d}t. \quad \text{(A7)}$$

$$\mathrm{d}f2(t) = 34936 \cdot \left(1.0 - 1.47 \times 10^{-3} \cdot F_{10.7}\right) (\sin \phi(t))^{5.80} \cdot fe2(t) \big/ (1.0 - fe2(t)) \quad \text{(A8)}$$

$$\cos \phi = \sin(fy \cdot t + 0.121) \cdot 0.0216 \cdot \sin(2\pi \cdot t - fy \cdot t - 1.29) + \cos(fy \cdot t + 0.121) \cdot (0.39 + 0.0236 \cdot \cos(2\pi \cdot t - fy \cdot t - 1.29)) \quad \text{(A9)}$$

$$fe2(t) = fe1(t) + (fe1(t - 0.0278) - fe1(t)) \cdot 0.156 \quad \text{(A10)}$$

$$fe1(t) = -8.276 \times 10^{-2} \cdot (B_t(t))^{1.39} \cdot (\sin \theta(t))^{6.92} \cdot (V_x(t)/430)^{4.17} \cdot \left(N_p(t)/7\right)^{0.23} \cdot \left[1 + \mathrm{erf}\left(0.039 \cdot \mathrm{d}h(t) \cdot B_p(t) \cdot \cos(\mathrm{ang}(t) + 0.06)\right)\right] \quad \text{(A11)}$$

$$\mathrm{d}h(t) = 1.65 \cdot \cos(fy \cdot t + 0.051) + \sin(2\pi \cdot t + 0.53), \quad \text{(A12)}$$

$$\mathrm{ang}(t) = \arctan\left(B_x(t), B_y(t)\right), \quad \text{(A13)}$$

A2. The *al*2

$$al2'(t) = 3.26 \cdot (\sin \phi(t - 0.0486))^{-6.93} \cdot B_z(t - 0.0486) \cdot (V_x(t - 0.0486)/430)^{0.56} \quad \text{(A14)}$$

$$al2''(t) = al2'(t) - |al2'(t)| \quad \text{(A15)}$$

$$al2(t) = \mathrm{smooth}^{15}\left(al2''(t), 3\right) \quad \text{(A16)}$$

A3. *P*_term

$$P_\text{term}(t) = -\left\{-0.483 \cdot (B_t(t))^2 \cdot \left(1 - 0.04 \cdot N_p(t)\right) + \left[3.22 \times 10^{-4} \cdot (\sin \phi(t))^{3.00} \cdot (V_x(t))^2 - 44.4\right] \cdot N_p(t)\right\}^{0.5} \quad \text{(A17)}$$

A4. *D*_term

$$D_\text{term}'(t) = 0.50 \cdot (B_z(t - 0.0597) - |B_z(t - 0.0597)|) \cdot (V_x(t - 0.0597)/500)^{0.74} \quad \text{(A18)}$$

$$D_\text{term}''(t) = \mathrm{smooth}^{39}\left(D_term'(t), 3\right) < -7.1 \quad \text{(A19)}$$

$$D_\text{term}(t) = -25.3 - 4.2 \cdot D_\text{term}''(t) \quad \text{(A20)}$$

A5. The *offset*

$$\text{offset} = (-0.0484 \cdot F_{10.7} - 1.26) \cdot (\sin \phi(t))^{-7.06} \quad \text{(A21)}$$

Appendix B: Correction to the Paper for Former *AL* Model

[44] In the paper, *Li et al.* [2007], there are three errors in their equations (12), (15), and (16). The correct form of equation (12) should read as follows:

$$a2(t) = a1(t)*(1.0 + 0.218*\sin(t*fy + 2.29)), \quad \text{(B1)}$$

the correct form of equation (15) should read

$$fe2(t) = fe1(t) + (fe1(t - 0.0347) - fe1(t))*0.077, \quad \text{(B2)}$$

and the correct form of equation (16) should read

$$fe1(t) = -5.529 \times 10^{-2} \cdot (B_t(t))^{1.530} \cdot (\sin \theta(t))^{6.51} \cdot (V_x(t)/430)^{4.10} \cdot \left(N_p(t)/7\right)^{0.170} \cdot \left[1 + \mathrm{erf}\left(0.0444 \cdot \mathrm{d}h(t) \cdot B_p(t) \cdot \cos(\mathrm{ang}(t) + 0.03)\right)\right]. \quad \text{(B3)}$$

None of the paper's results is affected by the correction.

[45] **Acknowledgments.** We appreciate the efforts of the science teams (WDC for Geomagnetism, Kyoto, Wind/3D, Wind/Mag, ACE/SWEPAM, ACE/Mag) in making data available. This work was mainly supported by NSF grant (ATM-0842388). It was also supported by the National Basic Research Programs of China (2011CB811406 and 2012CB825606). Bingxian Luo thanks Jiancun Gong for useful discussion and advices on the application of the models to real-time space weather forecasting.

[46] Robert Lysak thanks Alex Klimas and Tohru Araki for their assistance in evaluating this paper.

References

Ahn, B.-H., H. W. Kroehl, Y. Kamide, and E. A. Kihn (2000a), Universal time variations of the auroral electrojet indices, *J. Geophys. Res.*, *105*(A1), 267–275, doi:10.1029/1999JA900364.

Ahn, B.-H., H. W. Kroehl, Y. Kamide, and E. A. Kihn (2000b), Seasonal and solar cycle variations of the auroral electrojet indices, *J. Geophys. Res.*, *62*(14), 1301–1310, doi:10.1016/S1364-6826(00)00073-0.

Allen, J. H., and H. W. Kroehl (1975), Spatial and temporal distributions of magnetic effects of auroral electrojets as derived from AE indices, *J. Geophys. Res.*, *80*(25), 3667–3677, doi:10.1029/JA080i025p03667.

Bargatze, L. F., D. N. Baker, E. W. Hones Jr., and R. L. McPherron (1985), Magnetospheric impulse response for many levels of geomagnetic activity, *J. Geophys. Res.*, *90*(A7), 6387–6394, doi:10.1029/JA090iA07p06387.

Bargatze, L. F., R. L. McPherron, J. Minamora, and D. Weimer (2005), A new interpretation of Weimer et al.'s solar wind propagation delay technique, *J. Geophys. Res.*, *110*, A07105, doi:10.1029/2004JA010902.

Basu, S. (1975), Universal time seasonal variations of auroral zone magnetic activity and VHF scintillations, *J. Geophys. Res.*, *80*(34), 4725–4728, doi:10.1029/JA080i034p04725.

Berthelier, A. (1976), Influence of the polarity of the interplanetary magnetic field on the annual and the diurnal variations of magnetic activity, *J. Geophys. Res.*, *81*(25), 4546–4552, doi:10.1029/JA081i025p04546.

Cattell, C., J. Dombeck, M. Eskolin, L. Hanson, D. E. Lorshbough, C. W. Carlson, J. McFadden, and M. Temerin (2013), FAST observations of solar illumination and solar cycle dependence of the acceleration of upflowing ion beams on auroral field lines, *J. Geophys. Res. Space Physics*, *118*(6), 3203–3213, doi:10.1002/jgra.50302.

Chen, J., and A. S. Sharma (2006), Modeling and prediction of the magnetospheric dynamics during intense geospace storms, *J. Geophys. Res.*, *111*, A04209, doi:10.1029/2005JA011359.

Cliver, E. W., Y. Kamide, and A. G. Ling (2000), Mountains versus valleys: Semiannual variation of geomagnetic activity, *J. Geophys. Res.*, *105*(A2), 2413–2424, doi:10.1029/1999JA900439.

Davis, T. N., and M. Sugiura (1966), Auroral electrojet activity index AE and its universal time variations, *J. Geophys. Res.*, *71*(3), 785–801, doi:10.1029/JZ071i003p00785.

Gavrishchaka, V. V., and S. B. Ganguli (2001), Optimization of the neural-network geomagnetic model for forecasting large-amplitude substorm events, *J. Geophys. Res.*, *106*(A4), 6247–6258, doi:10.1029/2000JA900137.

Gleisner, H., and H. Lundstedt (1997), Response of the auroral electrojets to the solar wind modeled with neural networks, *J. Geophys. Res.*, *102*(A7), 14,269–14,278, doi:10.1029/96JA03068.

Gleisner, H., and H. Lundstedt (2001), Auroral electrojet predictions with dynamic neural networks, *J. Geophys. Res.*, *106*(A11), 24,541–24,550, doi:10.1029/2001JA900046.

Goertz, C. K., L.-H. Shan, and R. A. Smith (1993), Prediction of geomagnetic activity, *J. Geophys. Res.*, *98*(A5), 7673–7684, doi:10.1029/92JA01193.

Hernandez, J. V., T. Tajima, and W. Horton (1993), Neural net forecasting for geomagnetic activity, *Geophys. Res. Lett.*, *20*(23), 2707–2710, doi:10.1029/93GL02848.

Kamide, Y., and S. Kokubun (1995), Comment on "Substorm time constants" by D. R. Weimer, *J. Geophys. Res.*, *100*(A4), 5715–5718, doi:10.1029/94JA02931.

Kamide, Y., and G. Rostoker (2004), What is the physical meaning of the *AE* index?, *EOS Trans.*, *85*(19), 188–192, doi:10.1029/2004EO190010.

Klimas, A. J., D. N. Baker, D. A. Roberts, D. H. Fairfield, and J. Buechner (1992), A nonlinear dynamical analogue model of geomagnetic activity, *J. Geophys. Res.*, *97*(A8), 12,253–12,266, doi:10.1029/92JA00794.

Klimas, A. J., D. N. Baker, D. Vassiliadis, and D. A. Roberts (1994), Substorm recurrence during steady and variable solar wind driving: Evidence for a normal mode in the unloading dynamics of the magnetosphere, *J. Geophys. Res.*, *99*(A8), 14,855–14,862, doi:10.1029/94JA01240.

Lepping, R. P., et al. (1995), The wind magnetic field investigation, *Space Sci. Rev.*, *71*(1-4), 207–229, doi:10.1007/BF00751330.

Li, X., K. S. Oh, and M. Temerin (2007), Prediction of the AL index using solar wind parameters, *J. Geophys. Res.*, *112*, A06224, doi:10.1029/2006JA011918.

Li, X., M. Temerin, D. N. Baker, and G. D. Reeves (2011), Behavior of MeV electrons at geosynchronous orbit during last two solar cycles, *J. Geophys. Res.*, *116*, A11207, doi:10.1029/2011JA016934.

Lin, R. P., et al. (1995), A three-dimensional plasma and energetic particle investigation for the Wind spacecraft, *Space Sci. Rev.*, *71*(1-4), 125–153, doi:10.1007/BF00751328.

Luo, B., W. Tu, X. Li, J. Gong, S. Liu, E. Burin des Roziers, and D. N. Baker (2011), On energetic electrons (>38 keV) in the central plasma sheet: Data analysis and modeling, *J. Geophys. Res.*, *116*, A09220, doi:10.1029/2011JA016562.

Lyatsky, W., P. T. Newell, and A. Hamza (2001), Solar illumination as cause of the equinoctial preference for geomagnetic activity, *Geophys. Res. Lett.*, *28*(12), 2353–2356, doi:10.1029/2000GL012803.

McComas, D. J., S. J. Bame, P. Barker, W. C. Feldman, J. L. Phillips, P. Riley, and J. W. Griffee (1998), Solar Wind Electron Proton Alpha Monitor (SWEPAM) for the Advanced Composition Explorer, *Space Sci. Rev.*, *86*(1-4), 563–612, doi:10.1023/A:1005040232597.

Newell, P. T., T. Sotirelis, K. Liou, and F. J. Rich (2008), Pairs of solar wind-magnetosphere coupling functions: Combining a merging term with a viscous term works best, *J. Geophys. Res.*, *113*, A04218, doi:10.1029/2007JA012825.

Ober, D. M., N. C. Maynard, and W. J. Burke (2003), Testing the Hill model of transpolar potential saturation, *J. Geophys. Res.*, *108*(A12), 1467, doi:10.1029/2003JA010154.

Pulkkinen, T. I., E. I. Tanskanen, A. Viljanen, N. Partamies, and K. Kauristie (2011), Auroral electrojets during deep solar minimum at the end of solar cycle 23, *J. Geophys. Res.*, *116*, A04207, doi:10.1029/2010JA016098.

Rostoker, G. (2002), Why we have not yet solved the substorm problem, in *Proceedings of the Sixth International Conference on Substorms (ICS-6)*, edited by R. M. Winglee, p. 1, Univ. Wash., Seattle.

Rostoker, G., S.-I. Akasofu, J. Foster, R. A. Greenwald, A. T. Y. Lui, Y. Kamide, K. Kawasaki, R. L. McPherron, and C. T. Russell (1980), Magnetospheric substorms—Definition and signatures, *J. Geophys. Res.*, *85*(A4), 1663–1668, doi:10.1029/JA085iA04p01663.

Russell, C. T., and R. L. McPherron (1973), Semiannual variation of geomagnetic activity, *J. Geophys. Res.*, *78*(1), 92–108, doi:10.1029/JA078i001p00092.

Sharma, A. S., D. N. Baker, M. Grande, Y. Kamide, G. S. Lakhina, R. M. McPherron, G. D. Reeves, G. Rostoker, R. Vondrak, and L. Zelenyiio (2003), The storm-substorm relationship: Current understanding and outlook, in *Disturbances in Geospace: The Storm-Substorm Relationship, Washington DC American Geophysical Union Geophysical Monograph Series*, vol. 142, edited by A. S. Sharma et al., p. 1–14, AGU, Washington, D. C., doi:10.1029/142GM01.

Smith, C. W., J. L'Heureux, N. F. Ness, M. H. Acuña, L. F. Burlaga, and J. Scheifele (1998), The ACE magnetic fields experiment, *Space Sci. Rev.*, *86*(1-4), 613–632, doi:10.1023/A:1005092216668.

Takahashi, K., C. Meng, T. Kamei, T. Kikuchi, and M. Kunitake (2004), Near-real-time auroral electrojet index: An international collaboration makes rapid delivery of auroral electrojet index, *Space Weather*, *2*, S11003, doi:10.1029/2004SW000116.

Temerin, M., and X. Li (2002), A new model for the prediction of *Dst* on the basis of the solar wind, *J. Geophys. Res.*, *107*(A12), 1472, doi:10.1029/2001JA007532.

Temerin, M., and X. Li (2006), *Dst* model for 1995–2002, *J. Geophys. Res.*, *111*, A04221, doi:10.1029/2005JA011257.

Vassiliadis, D., A. J. Klimas, D. N. Baker, and D. A. Roberts (1995), A description of the solar wind-magnetosphere coupling based on nonlinear filters, *J. Geophys. Res.*, *100*(A3), 3495–3512, doi:10.1029/94JA02725.

Weigel, R. S., A. J. Klimas, and D. Vassiliadis (2003), Solar wind coupling to and predictability of ground magnetic fields and their time derivatives, *J. Geophys. Res.*, *108*(A7), 1298, doi:10.1029/2002JA009627.

Weimer, D. R. (1994), Substorm time constants, *J. Geophys. Res.*, *99*(A6), 11,005–11,016, doi:10.1029/93JA02721.

Weimer, D. R. (1995), Reply, *J. Geophys. Res.*, *100*(A4), 5719–5722, doi:10.1029/94JA02930.

Weimer, D. R., D. M. Ober, N. C. Maynard, M. R. Collier, D. J. McComas, N. F. Ness, C. W. Smith, and J. Watermann (2003), Predicting interplanetary magnetic field (IMF) propagation delay times using the minimum variance technique, *J. Geophys. Res.*, *108*(A1), 1026, doi:10.1029/2002JA009405.

Xu, W.-Y. (2009), Variations of the auroral electrojet belt during substorms, *Chinese J. Geophys.*, *52*(2), 301–310.